



Hydrothermal evolution in the Maher-Abad porphyry Cu–Au deposit, SW Birjand, Eastern Iran: Evidence from fluid inclusions



Kamal Siahcheshm^{a,*}, Ali Asghar Calagari^{a,1}, Ali Abedini^{b,2}

^a Department of Geology, Faculty of Natural Sciences, University of Tabriz, 5166616471, Tabriz, Iran

^b Department of Geology, Faculty of Sciences, University of Urmia, 57153165, Urmia, Iran

ARTICLE INFO

Article history:

Received 13 October 2013

Accepted 25 October 2013

Available online 2 November 2013

Keywords:

Fluid inclusions

Quartz-veinlets

Ore fluid evolution

Lithostatic pressure

Mixing

Cu–Au porphyry

Iran

ABSTRACT

Copper and gold mineralization in the Maher-Abad deposit, eastern Iran, is closely related to the multiple emplacement episodes of Upper Eocene granodiorite porphyries within andesitic volcanoclastic and coeval quartz monzonite stocks. The magmatic hydrothermal fluids thereafter hydrofracturing provided appropriate conduits, formed a stockwork of quartz and quartz–sulfide veinlets within the porphyritic host rocks which were extensively altered into potassic, propylitic, phyllic, and argillic assemblages. Four main vein/veinlet groups have been identified: (A) quartz ± K-feldspar ± biotite ± anhydrite with pyrite, chalcopyrite, sporadic magnetite and pyrrhotite; (B) quartz, pyrite and minor chalcopyrite; (C) chalcopyrite, quartz and/or minor bornite, pyrite, digenite and sporadic pyrrhotite; and (D) quartz, calcite and/or clay minerals ± pyrite ± hematite ± galena. The Cu–Au mineralization is mainly associated with the early potassic (biotite) alteration zone in the deep central part of the Madanha stock.

Based on the phase contents at room temperature, three types of fluid inclusions are recognized at Maher-Abad: (1) liquid-rich two-phase (LV), (2) vapor-rich (VL ± H) and (3) halite-bearing multiphase (LVH). Homogenization experiments revealed a temperature range of 150–488 °C for the studied inclusions. Ice-melting of aqueous two-phase inclusions and melting of halite in the aqueous multiphase inclusions provide salinity of 9.5 to 47.9 wt.% NaCl equivalent. Fluid-inclusion studies reveal that the single-phase low-salinity magmatic fluid, exsolved from a granodioritic magma, was separated into vapor and hypersaline brine (~45 wt.% NaCl eq.) phases. The coexisting phases were trapped at temperature 460 °C and lithostatic pressure of ~350 bars (corresponding to a depth of 1.3 km) as VL ± H and LVH fluid inclusions, respectively. Such magmatic-derived fluids underwent phase separation episodically under lithostatic pressure conditions and formed the early copper sulfide-bearing quartz veinlets intimately related to the potassic alteration zone. Copper–iron sulfide precipitation and phase separation concomitant of boiling in this zone led to rapid depletion of the fluid in reduced sulfur. As a result, Au(HS)₂⁻ complexes are destabilized forcing most of the gold to precipitate above 400 °C.

A positive trend of the homogenization temperature and salinity during the formation of the phyllic alteration zone is attributed to the cooling of a moderately saline fluid (produced dominantly by magmatic-vapor condensation) and its subsequent boiling and mixing with meteoric waters at a hydrostatic pressure of ~100–125 bars corresponding to a depth of ~1–1.2 km. The argillic alteration zone formed at temperature of 210–230 °C from fluids with salinity of 16–18 NaCl wt.% eq. at a hydrostatic pressure of ~80 bars and a depth of 800 m from paleo-surface. The fluid density is typically lower (<1 g/cm³) than that of the potassic zone (>1 g/cm³), indicating that the late trapped fluid was more dilute.

© 2013 Elsevier B.V. All rights reserved.

1. Introduction

The Maher-Abad porphyry Cu–Au deposit area is located ~70 km southwest of Birjand, Lut block, which is an extremely arid desert region in eastern Iran (Fig. 1a). An extensive Paleocene–Eocene arc magmatic suite occurs within the Lut block, just to the west of the Nehbandan

fault zone, where it crops out in arcuate, fault bounded mountain ranges (Fig. 1a). The Lut micro-continental block has significant potential for different types of mineralization, particularly porphyry Cu deposits, associated to subduction-related middle Eocene calc-alkaline porphyritic volcano-plutonic rocks (Richards et al., 2012). The Maher-Abad porphyry Cu–Au system with an average grade of the 0.15% Cu and 0.5 g t⁻¹ Au (Siahcheshm et al., 2012) is the only reported Cu–Au porphyry deposit located in the eastern part of the central Lut.

Three approaches are commonly used to constrain the characteristics of the ore-forming fluids: stable isotope geochemistry, fluid inclusion analyses, and mineral chemistry. The study of fluid inclusions in porphyry

* Corresponding author. Tel.: +98 411 3392699; fax: +98 411 3392703.

E-mail address: kl_siahcheshm@yahoo.com (K. Siahcheshm).

¹ Tel.: +98 411 3392699; fax: +98 411 3392703.

² Tel.: +98 441 2972134; fax: +98 441 2753172.

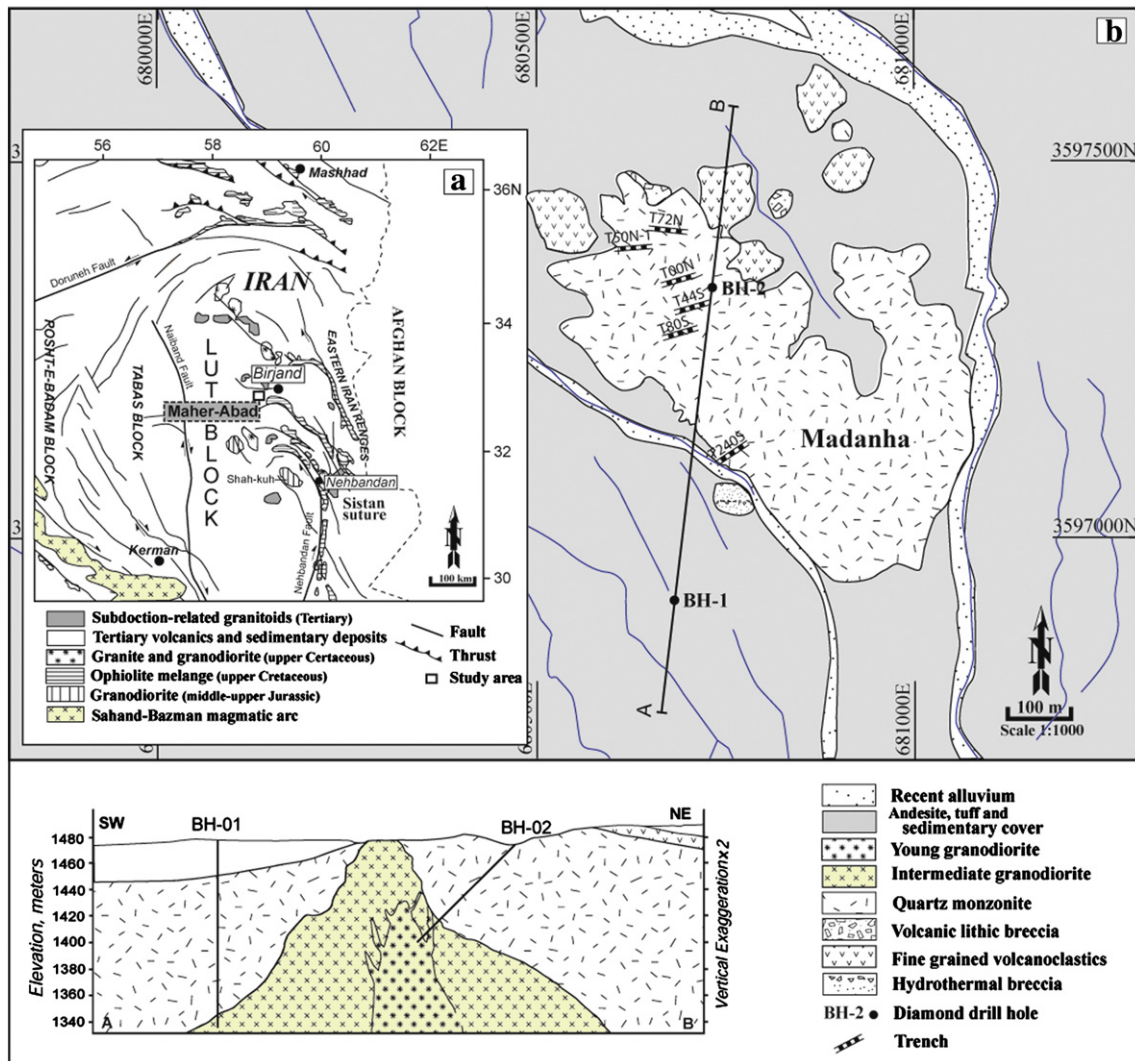


Fig. 1. (a) Structural map of Central–East Iran (after Ramezani and Tucker, 2003) and regional geological implications (compiled from Tarkian et al., 1983; Karimpour and Zaw, 2000; Karimpour et al., 2005). (b) Geological map of the Maher–Abad porphyry Cu–Au deposit with SW–NE geological section.

copper deposits is aimed to identify and characterize the pressure, temperature and fluid composition, (PTX) conditions of fluids under which they were trapped. The most comprehensive review of fluid inclusions have shown many common physico-chemical and genetic features in such deposits throughout the world e.g. the Copper Canyon, Nevada (Nash and Theodore, 1971); the Panguna, Papua New Guinea (Eastoe, 1978); the Santa Rita, New Mexico (Reynolds and Beane, 1985), the Sungun, Iran (Calagari, 2004) and the Miduk, Iran (Hezarkhani, 2008) and suggest a common mode of origin for these types of deposits. The host minerals (e.g., quartz) in veins/veinlets can trap different fluids with various compositions under different physico-chemical conditions prevailing during multiple fracturing events.

During of multiple events there may be different compositional fluids trapped within a single vein, which reflect some ambiguity in origin and evolution of low- and high-salinity fluid inclusions. For example, while low- to moderate-salinity fluids have been reported to be responsible for the formation of the early potassic alteration in a few deposits (e.g. Redmond et al., 2004; Rusk et al., 2008), in this study analogous to most porphyry-Cu deposits, we demonstrate that magmatic hydrothermal fluids from which high salinity fluid inclusions are derived caused Cu–Au mineralization associated with potassic alteration zone. Although high-salinity fluid inclusions are common in magmatic-fluid-related phyllic alteration in some deposits (e.g. Sungun; Calagari, 1997; El Salvador, Far Southeast, Panguna; Harris and Golding,

2002), abundances of low to moderate-salinity fluid inclusions trapped within late alteration-related veins/veinlets may depict mixing of a saline magmatic and low salinity meteoric waters (e.g. Beane and Bodnar, 1995; this study). This investigation is focused on a fluid inclusion study in quartz veins/veinlets associated with the early potassic, the transitional phyllic and the late argillic alteration zones of the Maher–Abad deposit. Detailed fluid inclusion microthermometry was conducted on quartz veins/veinlets at Maher–Abad to reconstruct temperature, pressure and compositions of magmatic–hydrothermal fluids during vein formation, wall rock alteration and metal precipitation during the life of a hydrothermal system. Maher–Abad deposit provides an excellent opportunity to explore the evolution of the ore-forming fluids through alteration zones and factors controlling Cu mineralization by integrating petrographic, mineralogic and fluid inclusion data within a known geologic framework.

2. Geologic setting

2.1. Regional geology

According to the classification of the structural units of Iran (Alavi, 1991; Berberian, 1981; Nabavi, 1976), the Maher–Abad porphyry Cu–Au deposit is located in the Lut block (Fig. 1a), which is in turn a part of

the Central Iran micro-continent and Alpine–Himalayan (Tethyan) orogenic belt (Ramezani and Tucker, 2003).

The paleotectonic setting of the Lut block is controversial and various scenarios have been proposed by different authors. The Central Iran micro-continent has similar sedimentary records in the Paleozoic as the Arabian platform and has been interpreted to share a common paleogeographic position close to the northern margin of Gondwanaland (Zarrinkoub et al., 2012). According to Lensch and Schmidt (1984), intensive orogenic movements during Mesozoic and Tertiary led to breaking and splitting of this platform, which resulted in a reactivation of different lineaments and finally Central Iran separated into various micro-continental blocks (Posht Badam, Tabas, Lut; see Fig. 1a) after collision with the Turan plate. Richards et al. (2012) argued that the numerous micro-continental and island-arc fragments are now compacted between multiple suture zones. The features of Late Cretaceous ophiolites and ophiolitic mélanges crop out along the Sistan suture zone (referred to as the Sistan Ocean separated the Lut and Afghan blocks), including Birjand and Nehbandan ophiolitic complexes (Fig. 1a) are summarized in Ghazi et al. (2004) and Moghadam et al. (2010).

The metamorphic basement of the Lut block has not been dated. Sedimentary strata in the Lut block are mainly younger than Permian and consist of shallow marine carbonates, shales and sandstones (Stöcklin et al., 1971). Continental Neogene sedimentary deposits and Quaternary sand dunes, salt flats and alluvial fans cover a large areas of the Lut block.

The widespread volcano-plutonic rocks of the Lut magmatic arc are the result of a west dipping subduction-related closure of the Neo-Tethys oceanic plate between the Lut and Afghan blocks in the Tertiary (Karimpour et al., 2005; Mazhari and Safari, 2013; Richards et al., 2012; Fig. 1a). Geological observations and Rb–Sr radiogenic isotope data indicate that the oldest magmatic activity in the Central Lut comprises mostly granites of post-early Jurassic (165–162 Ma) age (e.g. Shah-Kuh pluton; Esmaily et al., 2007; Tarkian et al., 1983; see Fig. 1a). Late Cretaceous adakitic granodiorites and early Eocene A-type granites were emplaced inside the Sistan suture zone (Zarrinkoub et al., 2012). The Cenozoic igneous activity in the Birjand area and vicinities commenced in the Middle Eocene by alkaline and shoshonitic volcanism (e.g. dacite of Kuh-e-Birg, 43 Ma; shoshonitic andesite of Qol-e-Gonbad, 39 Ma) continuing and climaxing during the Middle–Late Eocene as alkaline and calc-alkaline series (Karimpour et al., 2011). Magmatism continued through Eocene–Oligocene by emplacement of intermediate-acidic porphyritic intrusions (Mahmoudi et al., 2010). The area underlain by the Paleogene volcanics consists predominantly of andesites and dacites, and their pyroclastic equivalents (tuff and ignimbrite). The intrusive suites are lens-shaped characterized by variable age, size, and composition ranging from monzonite to granodiorite. Eruption of alkali basalts was active from the Mid-Miocene to Quaternary along the suture zone and the Nayband fault in western Lut region (Pang et al., 2012).

The hypabyssal Eocene–Oligocene plutonic rocks are generally associated with extensive copper–gold mineralization, representing Tertiary metallogenic episodes in the Lut block producing porphyry copper–gold, iron–oxide copper–gold (IOCG), vein-type and epithermal gold ore bodies, as well as many other sub-economic ones (Karimpour and Zaw, 2000; Karimpour et al., 2005; Tarkian et al., 1983).

The mineralized and altered rocks in the Maher-Abad area are hosted by three distinct elongate NW–SE trending stocks covering an area of approximately 6 km². They are covered by the volcanoclastic rocks. They range in composition from quartz monzonite to quartz monzodiorite. The most intensely mineralized zone comprises an area of 100 × 300 m occurring within a conical hill with a surface area of over 1500 × 1000 m, called the Madanha Hill (Fig. 1b). Further away (~300 m) from the Madanha Hill in SW direction, there is another intrusive body called Zardab Hill (with a surface expression 80 × 180 m). The hornblende-bearing quartz monzonite forms the dominant rock body. The third stock called MH3 Hill is located ~400 m to the west of Mahanha Hill. It

is to be noted, however, that the Zardab and MH3 stocks are not displayed in Fig. 1b.

2.2. Geology of the study area

The volcanic–plutonic evolution of the Maher-Abad deposit was initiated by the formation of an andesitic volcanoclastic succession during the lower to middle Eocene, consisting of fine-grained volcanoclastic and volcanic lithic breccia (Fig. 1b). The lithic clasts are commonly polymictic, subrounded to subangular and dominantly of volcanic origin. The andesitic volcanoclastic unit was intruded by a sub-volcanic porphyritic complex (as closely spaced stocks). The Madanha stock, with an age of 39 ± 0.8 Ma (U–Pb zircon; Malekzadeh, 2010), appears to be the largest pre-mineralization sub-volcanic intrusion within this area which intruded the almost coeval andesitic volcanoclastic rocks. These rock units are intruded by at least two texturally distinct phases of granodiorite porphyries which are referred to as “early granodiorite” and “late granodiorite”. The granodiorite porphyries form a north-northwesterly elongated stock in the central part of Madanha with a surface area extending over ~300 m². They form a steeply, west dipping cluster of closely spaced stocks, which form a crude conical mass, wider at depth and narrowing upward. However, only the early granodiorite is exposed at Maher-Abad (Fig. 1b). These intrusive phases are differentiated by their contact relationships, texture, abundance and size of quartz phenocrysts, groundmass characteristics, interception of veinlets, abundance of quartz (± sulfide) veinlets, and the overall copper–gold grade. However, the diagnostic criterion for distinguishing the granodiorite intrusive phases is their sharp contacts where earlier phase (early granodiorite) and related quartz–sulfide veinlets are truncated by the later phase. The early porphyry comprises closely spaced veins with intense K-alteration and substantial copper sulfides + pyrite ± magnetite. The late phase is characterized by more abundant rounded quartz phenocrysts (quartz-eyes), easily identifiable from the former because of infrequent veining and less intense alteration-mineralization. They distinctly cross-cut and offset the early porphyries and quartz veins/veinlets.

The copper and gold mineralization appears to be intimately affiliated to the emplacement of the early rather than the late porphyries those chiefly host sulfide minerals. The intrusive activity was terminated by emplacement of the late granodiorite (Siahcheshm et al., 2012).

2.3. Petrography of the granodiorite porphyries

Based on field and petrographic studies, copper and gold mineralization in the Maher-Abad area is thought to be closely related to the multiple-stage intrusion of granodiorite porphyries. The mineralogy of the early and the late granodiorite porphyries is almost identical, and includes phenocrysts (up to 40–50 vol.%) of plagioclase, hornblende, biotite and quartz (Table 1). The phenocrysts are set in a medium-grained groundmass of mainly quartz, K-feldspar, albite, and opaque minerals.

The plagioclase phenocrysts are predominantly euhedral–subhedral with complex compositional zoning varying systematically from An_{50–30} in the core to An_{30–2} near the rim. The hornblende phenocrysts are locally rimmed by biotite and partially replaced by secondary biotite flakes. The late granodiorite is less altered than the early stage and is readily identifiable by the presence of phenocrysts of medium-sized “quartz eye” and coarser (>2 mm in length) biotite and hornblende. Quartz phenocrysts are rounded and/or embayed, resulting likely from isothermal decompression of a water vapor-undersaturated magma (Whitney, 1989). The magmatic biotite phenocrysts are texturally euhedral to subhedral with reddish-brown to green color and range in size from 1 to 4 mm. These biotites are observed in both least-altered and altered samples (potassic and phyllic alteration zones), have phlogopitic composition with X_{Mg} ranging from 0.73 to 0.78 corresponding to a mole fraction of phlogopite ranging between 0.67 and

Table 2
Major vein/veinlet types and their characteristics in the Maher-Abad deposit.

Vein/veinlet	Mineral assemblages	Width (cm)	contact	Internal banding	Center line	Texture
A \cong	Qtz + Py + Cpy \pm Anh	<0.2	I	N	N	Gr
Ab	Qtz + Bt \pm Kf	<0.1	I	N	N	Gr
Ac	Qtz + Py + Cal	<1	I-R	Y	N	Gr
B	Qtz + Py \pm Chl	<6	R	Wk	Y	Gr-Dr
C	Py + Ccp + Bn \pm Po \pm Dg	<0.5	R	N	N	-
D	Cal + Qtz + Py \pm Hem \pm Ser \pm Gn	<0.8	R	Wk	N	Dr-Gr
Latest	Py	<0.4	R	N	N	-
	Cal	<1	R	N	N	Dr

Abbreviations: I = irregular, I-R = irregular-regular, Y = yes, N = no, WK = weak, Gr = granular and Dr = drusy.

0.2 cm), irregular wall-rock contacts (Fig. 2a) and granular texture (Table 2). The pygmatic characteristics of the veinlets suggest fracturing of a plastic rather than a brittle rock (cf. Brathwaite et al., 2001; Gustafson and Hunt, 1975; Muntean and Einaudi, 2001). The plastic nature of the veinlets may indicate their formation under lithostatic regime (Fournier, 1999). Locally the “Ac” veinlets exhibit irregular to regular wall-rock contacts with internal symmetry (Table 2, Fig. 2a–b).

3.2. B-veins/veinlets

They typically contain medium- to coarse-grained quartz \pm calcite, pyrite and minor chalcopyrite with sericite \pm chlorite selvages and generally cross-cut A-veinlets. They have 0.1 to 6 cm width, showing well-developed phyllic alteration haloes. These veins/veinlets exhibit continuous pattern with regular wall-rock contacts. Internal banding with fracture coating pyrite in the middle parts within the veins/veinlets is locally present (Table 2, Fig. 2c–d). According to Calagari et al. (2001) and Seedorff et al. (2005), this banding may result in multiple opening of quartz veins/veinlets and episodically introduction of fluid during evolution of the hydrothermal system.

3.3. C-veinlets

The chalcopyrite-bearing “C” veinlets consist of quartz and minor bornite, pyrite, digenite and sporadic pyrrhotite. Equant grains of magnetite are frequently observed and locally replaced by hematite on their rims. Most of copper and gold are contained in the A and/or C veinlets and associated with early alteration stage developed in the potassic as well as phyllic zones.

3.4. D-veinlets

The majority of these veinlets cross-cut all the previous veins/veinlets and consists of quartz, calcite \pm clay minerals (Fig. 2e–f) \pm hematite \pm galena. These veinlets are mostly associated with argillic alteration that overprints phyllic and propylitic assemblages. The only sulfide mineral is pyrite, which occupies about 15 vol.% of these veins. They are usually surrounded by narrow (<3 cm) envelopes of silicification. Continuous pattern, regular contacts and drusy texture, may suggest that the “D” veinlets formed by open-space filling under hydrostatic regime (cf. Fournier, 1999; Muntean and Einaudi, 2001).

4. Alteration and mineralization

Four main almost concentric shell-shaped hydrothermal alteration zones can be defined in the Maher-Abad deposit. They were developed in three temporally and spatially overlapping stages involving: (1) early, (2) transitional and (3) late. The early one consists of central potassic and peripheral propylitic alteration zones overprinting mineralized granodiorite also quartz monzonite and volcanoclastic andesitic wall rocks. The transitional and late alteration stages, referred to as “feldspar destructive alteration”, typically overprint the early stage alteration mineral assemblages.

The ore mineralization consists of the primary copper-bearing sulfides. The copper sulfides occur as disseminated grains in the groundmass and as fracture coatings associated with the early alteration mineral assemblage and quartz veinlets. The sulfides consist of chalcopyrite, digenite, and bornite. Gold occurs as inclusions within the sulfide grains. It is also present as free gold along quartz and/or silicate grain boundaries.

4.1. Potassic alteration

This zone occurs only at depth and does not crop out at surface. The altered granodiorite is typified by plagioclase, secondary biotite, quartz, pyrite, chalcopyrite and scattered magnetite. The medium-coarse-grained plagioclase is locally “dusted” by sericite of the later phyllic alteration (Table 1). The hydrothermal biotites commonly occur as aggregates of fine-grained flakes (typically 10–100 μ m) replacing the magmatic mafic minerals and/or present as disseminated flakes in the rock matrix and in veinlets. Typically the early potassically altered rock samples show brownish gray color reflecting the presence of abundant secondary biotite flakes (10–20%). The mineralization is manifested by the presence of hypogene copper-bearing sulfides which mostly occur as disseminated grains or associated with early to transitional “A”, “Ac” and “C” veinlets.

4.2. Propylitic alteration

The mineral assemblages within the propylitic alteration zone are typically characterized by replacement of mafic silicate phenocrysts and groundmass by chlorite and local epidote or calcite (Table 1). Replacement of plagioclase by calcite is quite common in this zone. In many samples the presence of sericite and chlorite without epidote may equate to the intermediate argillic (e.g. Ohio Creek; Brathwaite et al., 2001) which overprints phyllic and/or relicts of potassic alteration in the upper part of the Maher-Abad stockwork.

4.3. Phyllic alteration

The phyllic alteration is widely observed at surface outcrops as well as in the studied diamond drill cores and variably overprints earlier formed potassic and propylitic alterations (Fig. 9b). Quartz, sericite and chlorite (\pm minor calcite) constitute the phyllic alteration assemblage which is associated with pyrite (\pm Cu-sulfides) veins/veinlets at depth and with Cu-carbonates and Fe-hydroxides in supergene zone near the surface. This alteration occurs as selective and/or pervasive replacement.

4.4. Argillic alteration

The late argillic alteration is characterized by the nearly complete destruction and replacement of pre-existing mafic minerals (e.g. hornblende, biotite) and feldspars by fine to medium-grained white micas (i.e. sericite–paragonite), clay minerals (kaolinite, illite, montmorillonite),

quartz, and iron hydroxides. It also overlaps with the upper part of phyllic alteration zone where sericite and paragonite appear to coexist.

5. Fluid inclusion study

5.1. Analytical methods

Doubly polished thin sections (~100 μm thick) were prepared from 22 samples containing quartz veinlets from potassic, phyllic and argillic alteration zones for preliminary petrographic study. From these, six subsurface (taken from BH-2) and three surface samples containing representative populations of inclusions were then selected for microthermometric analysis using a Linkam TH600 heating–freezing stage attached to a Zeiss transmitted light microscope at the Institute of Mineralogy and Economic Geology, RWTH Aachen University, Germany. The stage was calibrated using synthetic inclusions of pure water at the freezing point (0 $^{\circ}\text{C}$) and critical point (374.1 $^{\circ}\text{C}$) and the triple point of carbon dioxide (–56.6 $^{\circ}\text{C}$). Fluid inclusion symbols and units presented in this study follow Diamond (2003) rules, as quantities are generally single letters set in an italic fonts (e.g. T, X, V, φ), processes always in upright subscripts (e.g. homogenization, melting) and phases and/or transitions (e.g. NaCl, ice, LV \rightarrow V) in regular fonts.

5.2. Petrography

The petrographical work identifies, describes and classifies fluid inclusions in quartz. Fluid inclusions in the Maher-Abad system are abundant in quartz of all vein types in different alteration zones, and range in diameter from 1 to 60 μm . The early quartz–sulfide veinlets in the potassic zone display fine-grained quartz crystals (width <2 mm) having

too small (<5 μm) fluid inclusions hence were chosen mainly for petrographic studies and some for micro-thermometric analyses.

Three major types of fluid inclusions are recognized in the analyzed quartz veins/veinlets on the basis of phase content at room temperature. Their essential features are as follows: (1) liquid-rich (LV), (2) vapor-rich (VL \pm H), and (3) halite-bearing multiphase (LVH).

LV inclusions are ubiquitous, with variable dimensions, up to 60 μm (mostly 5–20 μm) in diameter. The inclusion morphologies are commonly spheroidal, but locally they are tubular and irregular. In most cases the inclusions are recognized as secondary in origin, but a few of primary origin may also be present. The secondary ones are commonly localized along healed fracture planes that terminate at crystal boundaries (intra-granular trails; Fig. 3a, b) or extend across grain boundaries (trans-granular trails; Fig. 3e). The relationship of the inclusions along the crisscrossing planes reflects fluid introduction during repeated fracturing. The inclusions homogenize into liquid.

VL \pm H inclusions contain vapor + liquid \pm halite with no opaque minerals and various vapor fractions ranging from 60 to 90 vol.% (Fig. 3f). This type varies in size from 10 to 60 μm , with a common form of perfect negative quartz crystal shape (Fig. 3e). A few inclusions show equidimensional to elongate forms. These inclusions mainly homogenize to vapor, and rarely to liquid, or by critical behavior.

LVH inclusions are multiphase, and consist of liquid + vapor + halite + other solids. They have been further divided into two subtypes according to their homogenization behavior: 1) homogenized by vapor disappearance; 2) homogenized by daughter crystal dissolution. Common daughter minerals in LVH inclusions are mainly halite and rarely sylvite, hematite and an opaque mineral (possibly sulfide) (Fig. 3c,d). The VL \pm H and LVH inclusions are irregularly distributed or follow planes that terminate at quartz crystal boundaries, and could

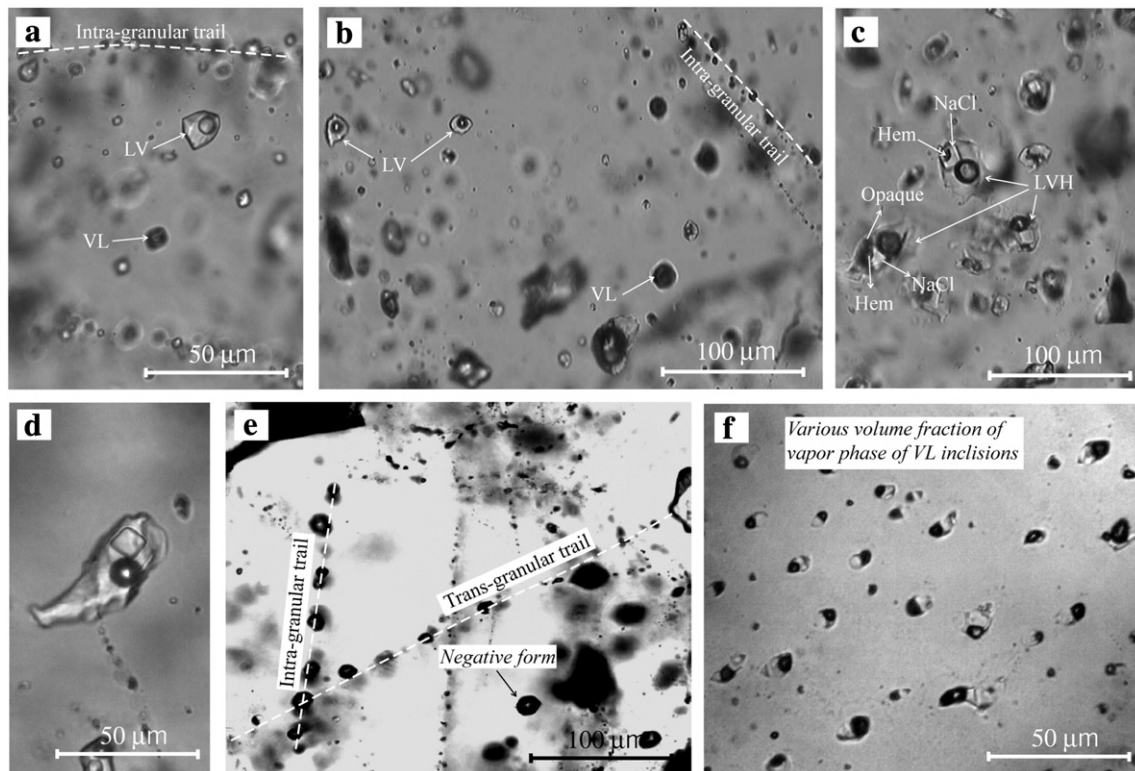


Fig. 3. Morphology of various types of fluid inclusions hosted in quartz vein/veinlets: (a, b) Spheroidal to irregular forms of secondary LV liquid-rich, VL \pm H vapor-rich as solitary inclusion or intra-granular trail, (c, d) Primary LVH inclusions with halite, hematite and other opaque daughter minerals. (e) Intra-granular VL \pm H fluid inclusions suggesting possibly pseudo-secondary origin, having perfect negative crystal form, and (f) Various volume fraction of vapor in VL \pm H inclusions. intra-granular and trans-granular terminology follows those of Kranz (1983); Vollbrecht (1989).

be primary or pseudo-secondary. However, these inclusion types are interpreted to represent the earliest episode of fluid entrapment in the system. Halite is generally larger than the other solids and can be readily distinguished by its cubic shape. Sylvite is smaller and has a rounded outline. The hematite daughter mineral typically shows orange-deep red color and dissolves on heating. All the inclusions analyzed at Maher-Abad were free of visible liquid CO₂.

5.3. Microthermometric analysis and results

Thermometric analyses were performed principally on fluid inclusions which were relatively large (>10 μm). Freezing was carried out mainly for halite-undersaturated inclusions, to determine the initial melting temperature (Te), the last melting point (Tm_{ice}) and salinity (wt% NaCl eq.), subsequently. During heating, the temperature of vapor and liquid homogenization were systematically measured on all types of inclusions. In the halite-bearing LVH inclusions, both Tm_{NaCl} and Th were recorded. However, the recorded Tm_{ice}, Tm_{NaCl} and/or Tm_{KCl} data were converted into corresponding salinity values by using AqSoVir software (Bakker, 2008a) using the equation for the H₂O–NaCl–[KCl] system. The fluid bulk density and bulk molar volume of inclusions are calculated using the Loner AP software (Bakker, 2008b) based on the relative volume ratios of liquid and vapor fractions at room temperature, and the known salinity.

In general, VL ± H inclusions with variable liquid–vapor ratios, gave inconsistent microthermometric data, with relatively high (generally >250 °C) and widely scattered Th values. This was interpreted as a consequence of heterogeneous trapping (Maineri et al., 2003). Clathrate formation was not observed in any of the fluid inclusions, which rules out the presence of significant CO₂.

5.3.1. Potassic alteration zone

Owing to the small size of many inclusions in fine-grained quartz veins/veinlets from the potassic alteration zone, phase changes recorded along low and high temperature runs could be only carried out on some inclusions. LV inclusions are relatively less abundant than the other two inclusion types.

- LV inclusions:** The microthermometric data of LV fluid inclusions from the potassic zone indicate that those homogenizing into liquid state have Th values varying from 298° to 361 °C (Fig. 4a). They particularly show a range of Te from –33° to –46 °C, which suggests at least the presence of species like MgCl₂ and FeCl₂ in the inclusions. The temperature of ice melting (Tm_{ice}) varies from –21° to –15 °C corresponding to an overall salinity of 15–22.4 wt.% NaCl eq. (Fig. 5a; Table 3).
- VL ± H inclusions:** Only two VL ± H inclusions could be measured, because of very poor visibility of the liquid phase and difficulty to determine the exact homogenization. The two VL ± H inclusions homogenize at 380° and 465 °C (Fig. 4a). Because of the small volume of liquid within these inclusions, it is difficult to measure Te. The first inclusion contains halite daughter crystal, with Tm_{NaCl} 330 °C, corresponding to 40.4 wt.% NaCl eq. The second fluid inclusion shows Tm (–20.1) and salinity of 20.2 wt.% NaCl eq. (Fig. 5a; Table 3). The VL ± H inclusions show a various volume fractions of the vapor phase.
- LVH halite-bearing inclusions:** The Th values for these inclusions range from 262° to 488 °C, with a well defined mode of 450° to 470 °C (Fig. 4a; Table 3). The halite melting temperature ranges from 290° to 405 °C, corresponding to an overall salinity of 37 to 48 wt.% NaCl eq. (~0.15–0.22 X_{NaCl}). The salinity versus frequency plot indicates that the salinity has a major peak at 44–46 wt.% NaCl eq. (Fig. 5a). Of all these inclusions, 75% homogenize by L–V homogenization after halite dissolution whereas the rest homogenize by halite dissolution above the temperature of L–V homogenization (Fig. 7). Three sylvite daughter minerals observed in the LVH

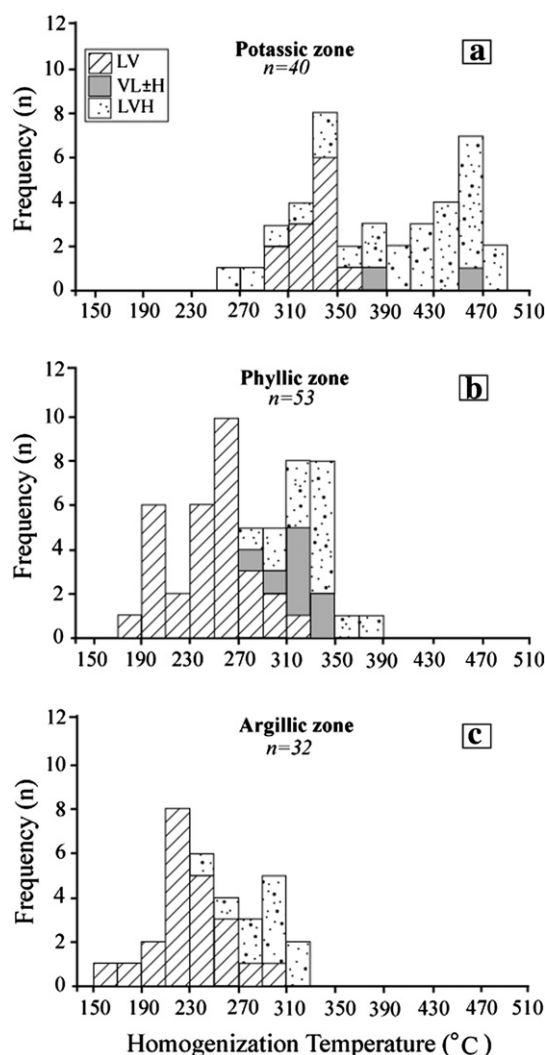


Fig. 4. Histograms of liquid–vapor homogenization temperatures for fluid inclusions from quartz veins/veinlets in different alteration zones.

inclusions indicate Tm_{KCl} from 104° to 126 °C; these are relatively lower than that of the halite crystals.

5.3.2. Phyllic alteration zone

The three types of fluid inclusions are identified within the veins/veinlets in this alteration zone, but LV ones are relatively more abundant than the other two types.

- LV inclusions:** The microthermometric analyses of LV inclusions indicate that the homogenization temperatures (Th) range from 181° to 315 °C and show two peaks: first at 250–270 °C and second at 190–210 °C (Fig. 4b). Te varies from –42° to –15.1 °C (suggesting the presence of FeCl₂ and/or MgCl₂ in addition to NaCl and KCl), with Tm_{ice} from –19.5° to –6.2 °C corresponding to salinity range of 9.5–22 wt.% NaCl eq. to NaCl mole fraction of 0.03–0.08 in the system. Fig. 5b displays two major peaks of salinity: 18–20 and 10–12 wt.% NaCl eq., respectively.
- VL ± H inclusions:** A total of 8 VL ± H inclusions have been analyzed, of which four contain halite daughter crystals, indicating higher salinity. The Tm_{NaCl} ranges from 260° to 320 °C (35.3–39.6 wt.% NaCl eq.). The inclusions with halite daughter crystals homogenize at temperatures of 285–347 °C, similar to LV inclusions (293–334 °C); (Fig. 4b). Inclusions without halite crystals exhibit intermediate salinity varying from 16.2 to 20 wt.% NaCl eq. (Fig. 5b).

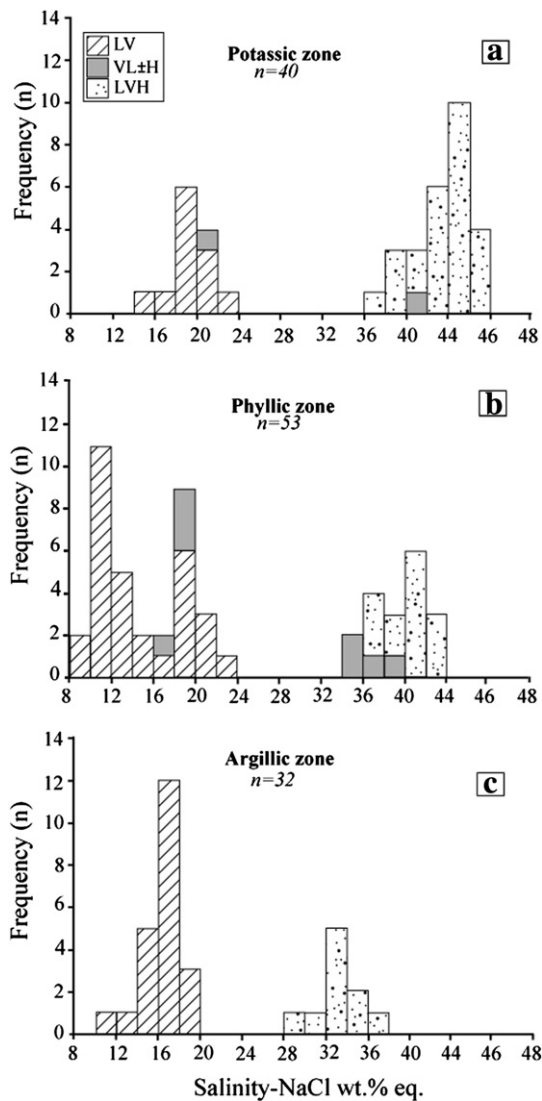


Fig. 5. Frequency plot of salinity (NaCl wt.% eq.) for fluid inclusions from quartz veins/veinlets in different alteration zones.

c) *LVH inclusions*: The liquid and vapor phases in LVH inclusions from the veins in the phyllic alteration zone homogenize to liquid at temperatures between 273° and 383 °C. The frequency distribution plot shows that the majority of the LVH inclusions homogenize at 330–350 °C (Fig. 4b). T_{mNaCl} ranges from 220° to 355 °C corresponding to salinities of 33–42.5 wt.% NaCl eq. (0.13–0.19

$X_{NaCl} \sim 4.8\text{--}14.2$ mol. NaCl) with a peak at 38–42 wt.% NaCl eq (Fig. 5b).

5.3.3. Argillic alteration zone

The LV liquid-rich inclusions, compared to VL ± H and LVH types are widely present. Most of (VL ± H) inclusions have variable liquid/vapor ratios, and may have formed by necking-down of halite-bearing inclusions or heterogeneous entrapment of liquid and vapor and have not been taken in account for the thermometric measurements.

- a) *LV inclusions*: These fluid inclusions homogenize to liquid at temperatures between 150° and 300 °C, with a well defined peak at 210–230 °C (Fig. 4c). The Th range is interpreted to be temperature of formation for the argillic alteration zone. Te varies from –36° to –11 °C suggesting multi-cation fluid that NaCl ± KCl are the principal salts in solution. T_{mice} ranges from –15.3° to –7 °C corresponding to salinities of 10.5–19 wt.% NaCl eq. (0.03–0.07 X_{NaCl}). The salinity histogram (Fig. 5c) indicates a salinity peak at 16–18 wt.% NaCl eq.
- b) *LVH inclusions*: The overall Th for the LVH type inclusions varies from 236° to 322 °C, with a peak of 290–310 °C (Fig. 4c). The T_{mNaCl} ranges from 145° to 265 °C, corresponding to salinity of 29.5 to 38 wt.% NaCl eq. The salinity has a major peak at 32–34 wt.% NaCl eq. (Fig. 5c). The hematite daughter minerals in the LVH fluid inclusions dissolve at temperature of ~304 °C, lower than Th ~322 °C (N = 2) which indicates that the hematite is indeed a daughter mineral (not a trapped solid).

6. Discussion

6.1. Th– T_{mice} –salinity relationships

As outlined above, three inclusion types (LV, VL ± H and LVH) are present in the quartz veins/veinlets associated with different alteration zones at Maher-Abad. The relationship between Th and T_{mice} as well as salinity of various fluid inclusion types in different alteration zones are illustrated in Fig. 6.

6.1.1. Potassic alteration zone

Two of the deepest samples (MA-B1-43 and MA-B1-47) from the quartz veinlets related to this alteration zone have been selected for microthermometric measurements. The early quartz veins/veinlets related to potassic alteration stage contain abundant LVH and low salinity VL ± H inclusions. The LVH inclusions homogenize mainly by disappearance of the vapor bubble at about 450–470 °C, following T_{mNaCl} at ~380–390 °C, equivalent to about 45 wt.% NaCl eq. In the sample (MA-B1-43) measurement of a VL ± H inclusion yielded liquid–vapor homogenization at 463 °C, whereas a nearby LVH inclusion homogenized at 459.3 °C. The similarity in the temperature of

Table 3
Summary of microthermometry data of fluid inclusions.

Alteration zones	Inclusion types	Size (µm)	Vol frac vap	T_{mice} (°C)	T_{mNaCl}	Th (°C)	Mode	Wt%NaCl	X_{NaCl}	Bulk den g/cm ³	Bulk MV cm ³ /mol
Potassic	LV (n = 12)	8–20	0.2–0.4	–11 to –20.1	–	298–361.5	L + V → L	14.98–22.4	0.05–0.08	0.82–1.03	20.54–24.53
	VL ± H (n = 2)	16–25	0.6, 0.7	–, –17 ^a	330, –	330,463	V + L ± S → V	20.2, 40.4	0.07, 0.17	0.70,1.04	23.94, 29.82
	LVH (n = 26)	12–28	0.3–0.4	–	290.5–405	262.3–488	L + V + S → L	37.3–47.9	0.15–0.22	0.99–1.15	22.2–25.1
Phyllic	LV (n = 31)	8–35	0.1–0.4	–6.2 to –19.5	–	181–315	L + V → L	9.5–22.0	0.03–0.08	0.77–0.99	19.7–25.2
	VL ± H (n = 8)	8–20	0.4–0.7	–12 to –17	260.4–320.2	285–347.2	V + L ± S → V	16.2–19.5	0.06–0.17	0.89–1.09	22.45–22.75
	LVH (n = 14)	12–28	0.1–0.3	–	220.7–355.2	273.2–383.1	L + V + S → L	33–42.5	0.13–0.18	0.97–1.10	22.78–24.16
Argillic	LV (n = 22)	8–35	0.1–0.4	–7 to –14.7	–	150.3–300.3	L + V → L	10.5–18.9	0.03–0.07	0.83–0.91	22.6–23.6
	LVH (n = 10)	12–28	0.2–0.3	–	145.2–297.4	236–322	L + V + S → L	29.6–37.9	0.11–0.16	0.99–1.07	22.42–22.97

All temperatures in °C. Salinity expressed as wt.% NaCl eq.

Vol Frac Vap = volume of vapor fraction; X_{NaCl} = mole fraction of NaCl; T_{mice} = temperature of final ice melting; Th = temperature of homogenization; Bulk Den = bulk density; Bulk MV = bulk molar volume of inclusions.

^a Not representative because of small number of measurements.

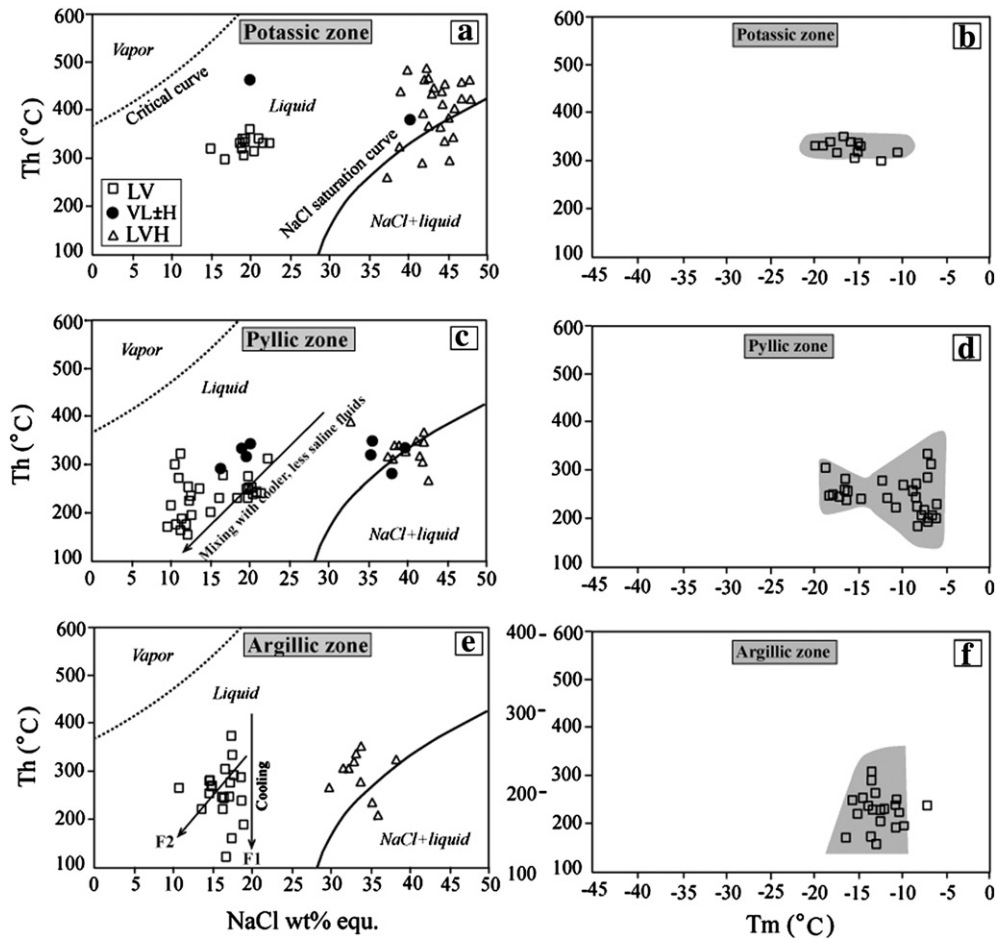


Fig. 6. Correlative plots for homogenization temperature (Th) against Salinity (wt.% NaCl eq.) and temperature of ice melting (Tm) of various fluid inclusion types within the Potassic (a–b), phyllic (c–d) and argillic (e–f) -related quartz veins/veinlets.

liquid–vapor homogenization of these two inclusion types supports the inference of the coeval fluid trapping. It suggests that the temperature of trapping (Tt) of the inclusions is equal to the Th at approximately 460 °C.

In the T_{mNaCl} versus Th plot of halite-bearing inclusions (Fig. 7), inclusions whose data points lie on and/or tightly around the diagonal line, when co-existing with vapor-rich inclusions homogenizing into

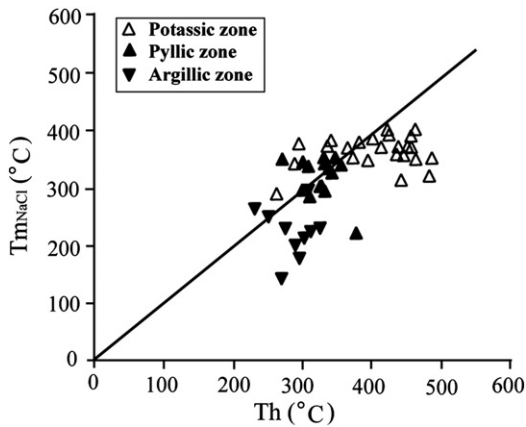


Fig. 7. Temperature of bubble homogenization (Th) versus temperature of halite dissolution (T_{mNaCl}) in LVH inclusions. The diagonal line is the line along which both halite and bubble homogenize at the same temperature. Of all inclusions, 75% plot above this line, indicating that halite dissolves before bubble homogenization.

a vapor state over the same Th, are considered to have trapped NaCl saturated immiscible fluid during boiling event (Shepherd et al., 1985).

6.1.2. Phyllic alteration zone

As discussed above the, three inclusion types are present in the quartz veins/veinlets associated with the phyllic alteration zone. The VL ± H and LVH inclusions are characterized by relatively high homogenization temperatures (330–350 °C) and salinities (38–42 wt.% NaCl eq.), which may suggest a minimal, if any, meteoric fluid influx. However, by continued boiling, resulting in increase of the salinity of residual fluid, cannot be ruled out (as is evident by the slightly horizontal arrays of the VL ± H and LVH data points below the halite saturation curve; Fig. 6c). The LV inclusions have a major peak of the Th ranges from 240° to 260 °C with a salinity of 18–20 wt.% NaCl eq. The Th of LV inclusions tend to be negatively correlated with Tm, and positively correlated with salinity (Fig. 6d–c, respectively). In contrast, the Th, Tm and salinity of VL ± H and LVH inclusions display a scatter distribution. A positive trend of the Th and salinity for LV inclusions may suggest that the hydrothermal fluids have been gradually mixed with cooler and less saline fluids (Shepherd et al., 1985; Fig. 6c).

At a temperature lower than 400 °C and a minimum pressure of about 5–25 MPa (hydrostatic pressure, depth of 0.5–2.5 km) liquid-rich lower temperature and salinity inclusions are commonly associated with phyllic alteration in porphyry copper deposits, and have been interpreted to represent mixed magmatic–meteoric fluids (Bean and Bodnar, 1995). However, Bodnar (1998) and Heinrich et al. (2004) have proposed on the basis of model calculations, that moderate to high temperature–salinity fluids and associate phyllic alteration formed

from condensation of magmatic vapor during the late stages of magma crystallization. This is consistent with the medium to high Th and salinity observed in LVH inclusions from the phyllic zone in the Maher-Abad deposit.

6.1.3. Argillic alteration zone

The determination of the temperature and salinity of fluids responsible for the formation of the argillic alteration is more reliable using the microthermometric data of the LV inclusions (cf. Gonzalez-Partida and Levresse, 2003; Hedenquist et al., 1998; Maineri et al., 2003 and Nash, 1976). On the basis of the frequency plots, the inclusions predominantly homogenize at 210–230 °C and have a salinity of 16–18 wt.% NaCl eq. The range is consistent with those of most argillic alterations in copper porphyry deposits (e.g. Th ~ 200–300 °C; salinity ~ 3–20 wt.% NaCl eq., at Bingham, Utah; Parry et al., 2002; Roedder, 1971). The low to moderate temperature and salinity may reflect a decrease of the temperature and salinity of the magmatic-derived fluids outward.

In the Th–salinity plot (Fig. 6e), the fluid shows two-stage evolution. The first stage relates to simple cooling fluid (F1), from a little above 300 °C with a scatter distribution of LV inclusions parallel to the Th axis followed by the late stage influx of cooler and less saline meteoric fluids (F2) (e.g. Mishra et al., 2005; Wilkinson, 2001).

Dubessy et al. (2003) have recently provided theoretical Th– $T_{m_{ice}}$ diagrams for different kinds of fluid mixing, by carrying out numerical modeling of mixing in the H₂O–NaCl system. Careful observation of the distribution of data points and their envelope give insights into temperature and salinity of mixing fluid end-members. In Fig. 6b, the identification of an alignment of data points sub-parallel to the compositional ($T_{m_{ice}}$) axis is an indication of isothermal mixing. However, by decreasing intensity of fracture porosity in lithostatic condition, data lie closer and closer to the near isothermal curve. Distribution of data points within Fig. 6d can be interpreted as a result of fluid mixing at a temperature intermediate between the fluid end-members and pressure fluctuations during mixing. The pattern generated from Fig. 6f, reveals a spread of data points parallel to the Th, which indicates pressure variations during trapping, such that the normal fluid regime was hydrostatic and fluid mixing was associated with occasional decrease in fluid pressure. The highest Th spread represents fluids, which have exchanged the maximum amount of heat with the host rock before trapping.

6.2. Pressure–depth estimates

The occurrence of vapor-rich or coexisting hypersaline liquid-rich inclusions and vapor-rich inclusions are a characteristic of boiling conditions (Bodnar, 1995; Hedenquist et al., 1998; Nash, 1976). If a boiling liquid and its coexisting vapor phase are trapped separately in a pair of inclusions, these two fluid inclusions will homogenize at the same temperatures, and the known pressure–temperature relation curve (Fournier, 1999; Redmond et al., 2004) can be used to determine the pressure of trapping (formation). Although being difficult, a pair of fluid inclusions within quartz vein sample (MA-B1-43) with the highest Th from the potassic zone was found to satisfy the requirements.

As described above, the “A” and/or “Ab” quartz (\pm sulfide) veinlets related to potassic alteration zone commonly show discontinuous pattern and irregular boundaries with the host rock suggesting that they underwent plastic deformation rather than brittle fracturing under lithostatic pressure (Fournier, 1999; Muntean and Einaudi, 2001). Assuming that the magmatic–hydrothermal system forming potassic alteration zone was predominantly under lithostatic pressure, using the pressure–temperature relation (e.g. Fournier, 1999; Redmond et al., 2004), the Tt of 460 °C and the salinity of 45 wt.% NaCl eq. correspond to the pressure of trapping of ~350 bars and depth of ~1.3 km beneath the Maher-Abad paleo-surface. It means that 460 °C, the maximum pressure for the coexistence of magmatic-derived fluids trapped in LVH and VL \pm H inclusions is approximately 350 bars under conditions that changed from lithostatic to hydrostatic (i.e., the fluid boiled episodically).

The phyllic-related “B” quartz veins/veinlets commonly show drusy texture, continuous pattern and a regular sharp contact with host rock. These characteristics may suggest that the veins/veinlets formed by open-space filling (Muntean and Einaudi, 2001), under a hydrostatic pressure (Eastoe, 1978; Hedenquist et al., 1998). The trapping temperature of 330–350 °C and salinity of 38–42 wt.% NaCl eq. correspond to a hydrostatic pressure of about 100–125 bars and a depth of ~1–1.2 km (cf. Fournier, 1999; Redmond et al., 2004).

The argillic-related “D” quartz veins/veinlets also typically display a drusy texture and locally brecciated, having a continuous pattern with regular wall-rock contacts. These veins/veinlets characteristics could be an evidence of open-space filling under a hydrostatic regime (cf. Gustafson and Hunt, 1975; Muntean and Einaudi, 2001). Assuming that the pressures within the argillic-related hydrothermal system were dominated by a hydrostatic regime, the Th (Tt) ranging from 210° to 230 °C and salinity of 16–18 wt.% NaCl eq. correspond to a pressure of ~80 bars and a depth of ~0.5 km. All analyzed samples indicate boiling conditions, thus, the estimated pressures are not necessary to be corrected.

6.3. Ore fluid evolution: constraints from microthermometric data

Fluid inclusions in quartz veins/veinlets related to the early potassic, the transitional phyllic and the late argillic alteration zones record the fluid evolution within the Maher-Abad deposit. Fig. 8 illustrates the evolution of the fluid (gray arrow) along an adiabatic cooling path, which is responsible for the formation of alteration zones.

The Al^{IV}-hornblende geobarometer (Anderson and Smith, 1995) calculation indicates that the mean pressure for the emplacement of the Maher Abad porphyries is approximately 1.4 ± 0.2 kbar, inferred to be crystallized at depths of about 5.5 km (Siahcheshm et al., 2012).

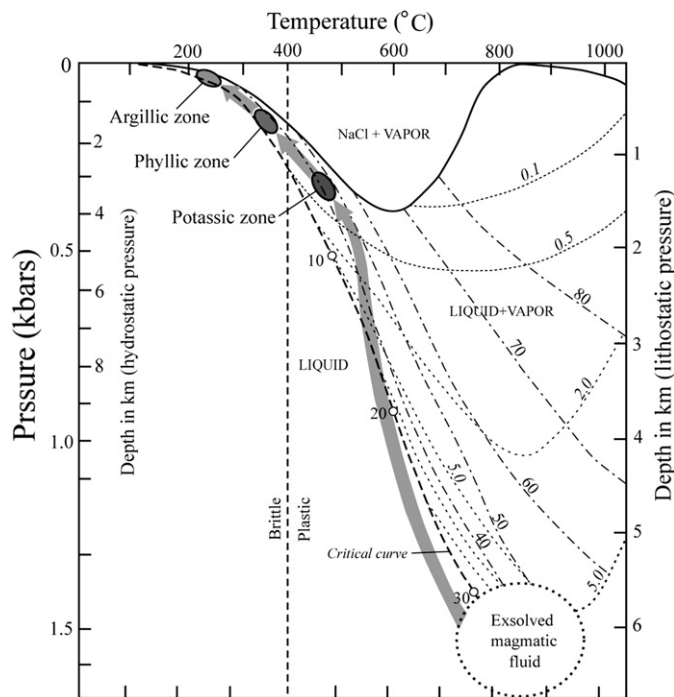


Fig. 8. Pressure–temperature (P–T) diagram for the H₂O–NaCl system (adapted from Fournier, 1999; Hedenquist et al., 1998; Redmond et al., 2004), showing the ascending path (gray arrow) for an exsolved aqueous magmatic fluid in the Maher-Abad deposit. The brittle plastic transition zone lies at about 400 °C (Fournier, 1999). The critical curve is shown by the dashed thick line with labels for 10, 20 and 30 wt.% NaCl eq. fluids. Dot-dashed lines are contours of constant wt.% NaCl dissolved in brine (boiling-point curves) with values for 30, 40, 50, 60, 70 and 80 wt. % NaCl eq. Dotted lines are contours of constant wt percent NaCl dissolved in vapor (condensation curves) with values for 0.1, 0.5, 2.0 and 5.0 wt.% NaCl eq., respectively.

The magma chamber at a depth of about 5.5 km was probably saturated with respect to water (H₂O) and other volatile components (e.g. CO₂, HCl and HF; cf. Burnham, 1979), and this led to exsolution of an aqueous fluid during crystallization of the initially convecting magma. The aqueous magmatic fluid can be represented by the system NaCl–H₂O and may exist as a single supercritical phase (Hedenquist, 1995). The cooling supercritical fluid would have intersected its solvus at ~460 °C (as determined in Sample MA-B1-43). As presented by Fournier (1999) at a depth less than ~5 km (<1300 bars), an exsolving magmatic fluid will dissociate immediately to high-salinity brine and steam. The ascending one-phase low salinity (<10 wt.% NaCl eq.) fluid underwent separation to vapor and hypersaline liquid/brine phases (Shinohara, 1994; Webster and Mandeville, 2007). If this single phase fluid breaches the L + V phases' surface on the liquid side of the critical curve, the fluid boils by separating out lower salinity vapor during ascend (cf. Heinrich et al., 2004). Thereafter, the coexisting vapor and hypersaline liquid phases were trapped in the VL ± H and LVH fluid inclusions, respectively, forming the early quartz veins/veinlets intimately related to the formation of the early potassic alteration which is directly associated with Cu and Au mineralisation in the Maher-Abad deposit. This zone occurs at a maximum temperature of about ~460 °C at depth of ~1.3 km under lithostatic pressure conditions supported by characteristics of the earliest "A" and "Ab" veinlets suggesting plastic rather than a brittle behavior.

The early mineralized potassic alteration zone may extend into the brittle–plastic transition which is determined on the basis of the observation of Fournier (1999) and commonly lies at temperatures of about 370° to 400 °C (Fig. 8). This fluid was responsible for the transport and eventual deposition of Cu, Fe, and S.

The ascent of the cooling granodiorite intrusions causes heating of the surrounding meteoric water beginning to circulate through the intrusions and wall-rocks (Fig. 9a). This may imply mixing of the magmatic–hydrothermal fluid with meteoric water up to several kilometers away from the intrusions similar to the fluid transport model of Norton (1978, 1982). Typically, temperature, pressure and salinity changes along the fluid flow paths produce dramatic changes in solvent properties (cf. Norton and Knight, 1977). As suggested by Beane and

Titley (1981), this model supports the interpretation that the VL ± H and LVH inclusions trap dominantly magmatic fluids, while LV inclusions trap mixed magmatic–meteoric fluids.

The first hydrothermal fluid was responsible for the transport and eventual deposition of copper sulfides. This fluid was characterized by high temperatures and moderate to high salinities, and was magmatically derived. It was responsible for the wide distribution of VL ± H and LVH inclusions and boiled episodically. The scattering of Th of these fluids (e.g. ranging from 260° to 490 °C in the potassic zone), is interpreted to represent heterogeneous entrapment, which suggests several boiling episodes correspond to potassic alteration in the deep part of the intrusion followed by copper mineralization and phyllic alteration in the upper part of the stock (e.g. Miduk-Iran, Hezarkhani, 2008).

The mixing of both fluids is illustrated by a systematic decrease of homogenization temperature and salinity (Fig. 6c, 5e). The homogenization temperature decreases from 383° to 273 °C for the outer phyllic alteration, and 300° to 150 °C for the argillic alteration. The salinity decreases from 42.5 to 33 wt.% NaCl eq. for the phyllic alteration, and 19 to 10.5 wt.% NaCl eq. for the argillic alteration. The changes in fluid temperature and salinity reflect the cooling of a saline fluid, produced dominantly by magmatic-vapor condensation (Heinrich et al., 2004), and its subsequent phase separation and mixing with meteoric waters as pressure conditions evolved being dominantly lithostatic in the potassic alteration zone, to dominantly hydrostatic in the phyllic and argillic alteration zones (cf. Bowman et al., 1987; Shepherd et al., 1985; Ulrich et al., 2001, 2002). The evidence of boiling, as described above, is the coexisting of hypersaline LVH and VL ± H vapor-rich inclusions, which show a various volume fraction of vapor phase, homogenizing over the same temperature range.

Between the large number of factors that may cause gold precipitation, phase separation has been suggested to explain the formation of high-grade ore zones in many deposits (Robert and Kelly, 1987; Walsh et al., 1988). More commonly in porphyry-style Cu–Au mineralization, initially the single-phase magmatic fluids contain a slight excess of chalcophile metals (e.g. Fe, Cu and possibly Au) relative to sulfur (cf. Burnham and Ohmoto, 1980). Similarly, the precipitation of pyrite, chalcopyrite, and bornite causes rapid depletion of reduced S in the

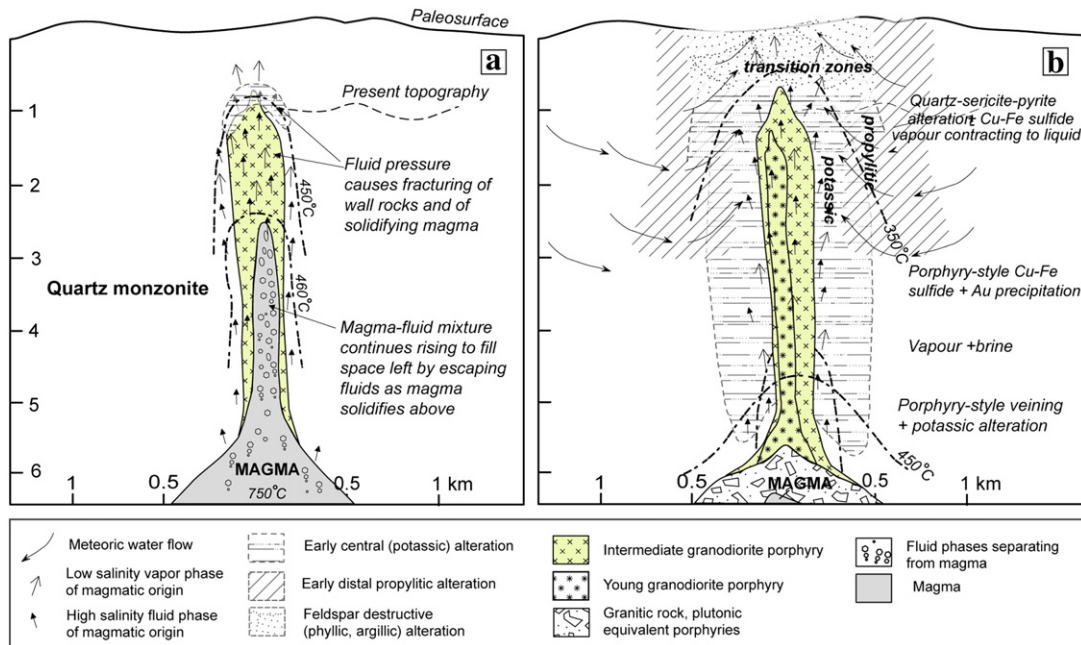


Fig. 9. Two stages in evolution of the Maher-Abad Cu–Au porphyry deposit. a) Vapor and hypersaline liquid phases were separated from the single-phase magmatic fluid at ~460 °C, ~2.2 km below the paleosurface. b) The early central biotite (potassic) alteration zone begins to form, which is associated with high Cu and Au mineralisation. Downward retraction of magma interface and surrounding isotherms occur during cooling and mixing with meteoric waters documented by fluid inclusions microthermometry.

magmatic fluid exsolved from the Maher-Abad granodioritic. Consequently, gold bisulfide complexes $[\text{Au}(\text{HS})_2^-]$ are destabilized, forcing most of the gold to precipitate above 400 °C, in the potassic alteration zone of the Maher-Abad deposit. Therefore, invariable occurrence of gold associated with sulfides, even in the quartz veins, indicating that sulfide precipitation and phase separation concomitant of boiling were major controlling factors for gold and sulfide precipitation in quartz veins associated with the potassic alteration zone.

As the intrusion cools (Fig. 9b), the region of brine + vapor coexistence above the magma interface retracts downward, leading to porphyry-style Cu-Au mineralization and potassic alteration by cooling of the ascending two-phase fluid through the 400–350 °C (e.g. Redmond et al., 2004; Ulrich et al., 2001).

The evidence for a hydrostatic-dominated pressure regime responsible for the formation of the phyllic and argillic alteration zones is illustrated by the drusy of their-related quartz veins/veinlets, showing continuous pattern (lengths greater than tens of centimeters) with regular contacts. The characteristics of the veins/veinlets suggest an open-space filling under brittle conditions.

Late fractures, or reopened veins, provided pathways for a fluid of mainly mixed meteoric and magmatic origin to circulate in the system at moderate to low temperatures. It is proposed that at temperatures around 340 °C, partial boiling and subsequent mixing with meteoric fluids caused the variation in salinity. This fluid was responsible for the phyllic alteration formation in the upper portion of the stock and argillic alteration in regions where it penetrated into the system (e.g. Hezarkhani, 2008). The density of the fluid is typically low ($<1 \text{ g/cm}^3$) relative to the fluid density related to the potassic alteration zone ($>1 \text{ g/cm}^3$), which suggests that the fluid related to the argillic alteration is more dilute resulted from the inflow of low salinity heated meteoric waters during cooling of the system.

7. Conclusions

The fluid inclusions within the quartz veins/veinlets record the physico-chemical evolution of fluids at the Maher-Abad copper–gold porphyry deposit. The coexisting vapor and hypersaline liquid phases continued to ascend and trapped in the VL \pm H and LVH fluid inclusions, respectively. The early-transitional quartz veins/veinlets contain abundant vapor-rich and hypersaline (~45 wt.% NaCl eq.) liquid-rich inclusions. The inclusions were trapped together in the VL \pm H and LVH inclusions, respectively, at a temperature of about 460 °C and a lithostatic pressure of 350 bars at a paleo-depth of ~1.3 km. These inclusions, are inferred to have separated from magmatic–hydrothermal fluids and co-genetic as an indication of boiling conditions. The cooling pluton provided heat supply required during the boiling event that recurred episodically (between 460 and 210 °C, Fig. 6) resulting in multi-phase hydro-fracturing events. It is proposed that during repeated cracking and sealing of the existing fractures by the precipitation of quartz, (\pm sulfides and carbonates), fluid pressure generally oscillated and exceeded lithostatic pressure, thereby, multiple episode of shattering and concomitant release of fluid and boiling took place in different places in the Maher-Abad deposit. The estimated trapping conditions for the fluid inclusions represent a minimum pressure, temperature and salinity and depth for conditions that prevailed during precipitation of early copper sulfide-bearing quartz veins/veinlets associated with the early potassic alteration in the core of the deposit.

The earliest quartz (\pm sulfide) veinlets related to potassic zone having plastic behavior rather than brittle may indicate their formation under lithostatic regime. The evidence for a hydrostatic-dominated pressure regime responsible for the formation of the phyllic and argillic alteration zones is exhibited by open-space filling under brittle conditions. It is suggested that the $\text{Au}(\text{HS})_2^-$ complex was the dominant complex in the fluids during mineralization and gold deposition. Destabilization of gold bisulfide complex was mainly induced by phase separation and sulfidization of wall rocks. The LV inclusions are more

abundant than the other types in quartz veins/veinlets related to the phyllic and argillic alterations zones, which may depict the increase of the flow influx from the central to the peripheral parts of the deposit. The decrease of temperature and salinity of the magmatic-derived fluids outward may also be attributed to the late stage mixing of meteoric fluids.

The fluids forming the phyllic alteration are characterized by relatively high homogenization temperatures (330–350 °C) and salinities (38–42 wt.% NaCl eq.). The hydrostatic pressures of about 100–125 bars correspond to the paleo-depth of about 1–1.2 km, representing upper part of the potassic alteration.

The more dilute fluids (density ~0.85–0.99 g/cm^3) associated with the argillic alteration are estimated to have been trapped within the late quartz veins/veinlets at temperatures of 210–230 °C and a salinity of 16–18 wt.% NaCl eq. The pressures of trapping were under a hydrostatic regime at about 80 bars, which corresponds to a paleo-depth of ~800 m.

Acknowledgements

This contribution is a part of the first author's PhD thesis, the laboratory studies were carried out at the Institute of Mineralogy and Economic Geology, RWTH Aachen University, Germany. Funding for this project was provided by the Ministry of Science, Research and Technology, Iran. My grateful appreciation is extended to Dr. Christoph Piribauer for his assistance in fluid inclusion laboratory. The original manuscript was improved by thoughtful and insightful reviews from Kalin Kouzmanov and Hadi Shafaii Moghadam along with the editorial help rendered by Prof. Franco Pirajno and Prof. Nigel Cook.

References

- Alavi, M., 1991. Tectonic map of the Middle East (scale 1:5,000,000). Geological Survey of Iran.
- Anderson, J.L., Smith, D.R., 1995. The effects of temperature and f_{O_2} on the Al-hornblende barometer. *Am. Mineral.* 80, 549–559.
- Bakker, R.J., 2008a. AqSoVir software package fluids, v. 2. Fluid inclusion laboratory Leoben, for fluid system: H₂O–NaCl–KCl–CaCl₂ (partly). <http://fluids.unileoben.ac/computer.html>.
- Bakker, R.J., 2008b. Loner Ap software package fluids, v. 2. Fluid inclusion laboratory Leoben, for fluid system: H₂O–CO₂–CH₄–NaCl–KCl. <http://fluids.unileoben.ac/computer.html>.
- Beane, R.E., Bodnar, R.J., 1995. Hydrothermal fluids and hydrothermal alteration in porphyry copper deposits. In: Pierce, F.W., Bohm, J.G. (Eds.), *Porphyry copper deposits of the American Cordillera: Tucson, AZ, Arizona Geological Society Digest*, 20, pp. 83–93.
- Beane, R.E., Titley, S.R., 1981. Porphyry copper deposits. Part II: Hydrothermal alteration and mineralization. *Econ. Geol.* 75th anniversary volume, pp. 235–269.
- Berberian, M., 1981. Active faulting and tectonics of Iran. In: Gupta, H.K., Delany, F.M. (Eds.), *Zagros-Hindu Kush-Himalaya Geodynamic Evolution. American Geophysical Union Geodynamic Series*, 3, pp. 33–69.
- Bodnar, R.J., 1995. Fluid inclusion evidence for a magmatic source for metals in porphyry copper deposits. In: Thompson, J.F.H. (Ed.), *Mineralogical Association of Canada Short Course, Magmas, Fluids and Ore Deposits*, vol. 23, pp. 139–152.
- Bodnar, R.J., 1998. A model for the temporal and spatial evolution of magmatic fluid inclusion in porphyry copper deposits. *PACROFI VII, Pan-American Conference on Research on Fluid Inclusions, Program and Abstracts. New Bur Mines Geol Open-File Rep* 98-4:16.
- Bowman, J.R., Parry, W.T., Kropp, W.P., Krueger, S.A., 1987. Chemical and isotopic evolution of hydrothermal solutions at Bingham, Utah. *Econ. Geol.* 82, 395–428.
- Brathwaite, R.L., Simpson, M.P., Faure, K., Skinner, D.N.B., 2001. Telescoped porphyry Cu–Mo–Au mineralization, advanced argillic alteration and quartz-sulphide-gold-anhydrite veins in the Thames district, New Zealand. *Miner. Deposita* 36 (7), 623–640.
- Burnham, C.W., 1979. Magmas and hydrothermal fluids. In: Barnes, H.L. (Ed.), *Geochemistry of Hydrothermal Ore Deposits: New York. John Wiley and Sons, United States*, pp. 71–136.
- Burnham, C.W., Ohmoto, H., 1980. Late-stage processes of felsic magmatism. In: Ishihara, S., Takenouchi, S. (Eds.), *Granitic Magmatism and Related Mineralization: Tokyo, Japan. Mining Geology Special Issue*, 8, pp. 1–11.
- Calagari, A.A., 1997. Geochemical, stable isotope, noble gas and fluid inclusion studies of mineralization and alteration at Sungun porphyry copper deposit, East-Azarbaidjan, Iran: Implication for genesis. Unpublished Ph.D. Thesis, Manchester University, 537 p.
- Calagari, A.A., 2004. Fluid inclusion studies in quartz veinlets in the porphyry copper deposit at Sungun, East-Azarbaidjan, Iran. *J. Asian Earth Sci.* 23, 179–189.
- Calagari, A.A., Patrick, R.A.D., Polya, D.A., 2001. Veinlets and microveinlets studies in Sungun porphyry copper deposit, East-Azarbaidjan, Iran. *Q. J. Geosci. Geol. Surv. Iran* 10 (39–40), 70–79.

- Diamond, L.W., 2003. Glossary: Terms and Symbols used in Fluid Inclusion Studies. In: Samson, I., Anderson, A., Marshall, D. (Eds.), *Fluid Inclusions, Analysis and Interpretation*. Short Course, 32. Mineralogical Association of Canada, pp. 365–374.
- Dubessy, J., Derome, D., Sausse, J., 2003. Numerical modelling of fluid mixings in the H₂O–NaCl system application to the North Caramal U prospect (Australia). *Chem. Geol.* 102, 1–15.
- Eastoe, C.J., 1978. A fluid inclusion study of the Panguna porphyry copper deposit, Bougainville, Papua New Guinea. *Econ. Geol.* 73, 721–748.
- Esmaily, D., Bouchez, J.L., Siqueira, R., 2007. Magnetic fabrics and microstructures of the Jurassic Shah-Kuh granite pluton (Lut Block, Eastern Iran) and geodynamic inference. *Tectonophysics* 439, 149–170.
- Fournier, R.O., 1999. Hydrothermal processes related to movement of fluid from plastic into brittle rock in the magmatic-epithermal environment. *Econ. Geol.* 94, 1193–1211.
- Ghazi, A.M., Hassanipak, A.A., Mahoney, J.J., Duncan, R.A., 2004. Geochemical characteristics, ⁴⁰Ar–³⁹Ar ages and original tectonic setting of the Band-e-Zeyarat/Dar Anar ophiolite, Makran accretionary prism, S.E. Iran. *Tectonophysics* 393, 175–196.
- Gonzalez-Partida, E., Levresse, G., 2003. Fluid inclusion evolution at the La Verde porphyry copper deposit, Michoacan, Mexico. *J. Geochem. Explor.* 78–79, 623–626.
- Gustafson, L.B., Hunt, J.P., 1975. The porphyry copper deposit at El Salvador, Chile. *Econ. Geol.* 70, 857–912.
- Harris, A.C., Golding, S.D., 2002. New evidence of magmatic-fluid-related phyllic alteration: Implications for the genesis of porphyry Cu deposits. *Geology* 30 (4), 335–338.
- Hedenquist, J.W., 1995. The ascent of magmatic fluid: discharge versus mineralization. *Short Course Series, 23*. Mineralogical Association of Canada, pp. 263–289.
- Hedenquist, J.W., Arribas, A., Reynolds, T.J., 1998. Evolution of an intrusion centered hydrothermal system: Far Southeast–Lepanto porphyry and epithermal Cu–Au deposits, Philippines. *Econ. Geol.* 93, 373–404.
- Heinrich, C.A., Driessner, T., Stefansson, A., Seward, T.M., 2004. Magmatic vapor contraction and the transport of gold from the porphyry environment to epithermal ore deposits. *Geology* 32, 761–764.
- Hezarkhani, A., 2008. Hydrothermal evolution of the Miduk porphyry copper system, Kerman, Iran: a fluid inclusion investigation. *Int. Geol. Rev.* 50, 665–684.
- Karimpour, M.H., Zaw, K., 2000. Geochemistry and physicochemical condition of Qaleh-Zari Cu–Ag–Au ore bearing solution based on chlorite composition. *Iran. J. Crystallogr. Mineral.* 8, 3–22.
- Karimpour, M.H., Zaw, K., Huston, D.L., 2005. S–C–O isotopes, fluid inclusion microthermometry, and the genesis of ore bearing fluids at Qaleh-Zari Fe–Oxide Cu–Au–Ag Mine, Iran. *J. Sci. Islam. Repub. Iran* 16 (2), 153–169.
- Karimpour, M.H., Stern, C.R., Farmer, L., Saadat, S., Malekzadeh, A., 2011. Review of age, Rb–Sr geochemistry and petrogenesis of Jurassic to Quaternary igneous rocks in Lut Block, Eastern Iran. *J. Geopiersia* 1, 19–36.
- Kranz, R.L., 1983. Micro-cracks in rocks: a review. *Tectonophysics* 100, 449–480.
- Lensch, G., Schmidt, K., 1984. Plate tectonic, orogeny, and mineralization in the Iranian fold belts results and conclusions. *N. Jb. Geol. Palaont. Abh.* 168 (2/3), 558–568.
- Mahmoudi, S., Masoudi, F., Corfu, F., Mehrabi, B., 2010. Magmatic and metamorphic history of the Deh–Salm metamorphic Complex, Eastern Lut block, (Eastern Iran), from U–Pb geochronology. *Int. J. Earth Sci.* 99, 11153–11165.
- Maineri, C., Benvenuti, M., Costagliola, P., Dini, A., Lattanzi, P., Ruggieri, G., Villa, I.M., 2003. Sericitic alteration at the La Crocetta deposit (Elba Island, Italy): interplay between magmatism, tectonics and hydrothermal activity. *Miner. Deposita* 38, 67–86.
- Malekzadeh, A., 2010. Rb–Sr and Sm–Nd isotopic compositions and Petrogenesis of ore-related intrusive rocks of gold-rich porphyry copper Maherabad prospect area (North of Hanich), east of Iran. *Iran. J. Crystallogr. Mineral.* 18, 15–32.
- Mazhari, S.A., Safari, M., 2013. High-K calc-alkaline plutonism in Zouzan, NE of Lut block, Eastern Iran: an evidence for arc related magmatism in Cenozoic. *J. Geol. Soc. India* 81, 698–708.
- Mishra, B., Pal, N., Sarbadhikari, A.B., 2005. Fluid inclusion characteristics of the Uti gold deposit, Hutti–Maski greenstone belt, southern India. *Ore Geol. Rev.* 26, 1–16.
- Moghadam, H.S., Stern, R.J., Rahgoshay, M., 2010. The Dehshir ophiolite (central Iran): geochemical constraints on the origin and evolution of the Inner Zagros ophiolite belt. *Geol. Soc. Am. Bull.* 122, 1516–1547.
- Muntean, J.L., Einaudi, M.T., 2001. Porphyry-epithermal transition: Maricunga Belt, Northern Chile. *Econ. Geol.* 96, 743–772.
- Nabavi, M., 1976. An Introduction to the Geology of Iran. Geological Survey of Iran Publication (in Persian 109 pp.).
- Nash, J.T., 1976. Fluid inclusion petrology, data from porphyry copper deposits and applications to exploration. United States Geological Survey, Professional Paper, 907-D, pp. 1–16.
- Nash, J.T., Theodore, T.G., 1971. Ore fluids in the porphyry copper deposit at Copper Canyon, Nevada. *Econ. Geol.* 66, 385–399.
- Norton, D.L., 1978. Source lines, source regions, and path lines for fluids in hydrothermal systems related to cooling plutons. *Econ. Geol.* 73, 21–28.
- Norton, D.L., 1982. Fluid and heat transport phenomena typical of copper-bearing pluton environments; southeastern Arizona. In: Titley, S.R. (Ed.), *Advances in Geology of Porphyry Copper Deposits; Southwestern North America*: Tucson, AZ. University Arizona Press, United States, pp. 59–72.
- Norton, D., Knight, J.E., 1977. Transport phenomena in hydrothermal systems; cooling plutons. *Am. J. Sci.* 277, 937–981.
- Pang, K.N., Chung, S.L., Zarrinkoub, M.H., Mohammadi, S.S., Yang, H.M., Chu, C.H., Lee, H.Y., Lo, C.H., 2012. Age, geochemical characteristics and petrogenesis of Late Cenozoic intraplate alkali basalts in the Lut-Sistan region, eastern Iran. *Chem. Geol.* 306–307, 40–53.
- Parry, W.T., Jasumback, M., Wilson, P.N., 2002. Clay mineralogy of phyllic and intermediate argillic alteration at Bingham, Utah. *Econ. Geol.* 97, 221–239.
- Ramezani, J., Tucker, R., 2003. The Saghand region, central Iran: U–Pb geochronology, petrogenesis and implications for Gondwana tectonics. *Am. J. Sci.* 303, 622–665.
- Redmond, P.B., Einaudi, M.T., Inan, E.E., Landtwing, M.R., Heinrich, C.A., 2004. Copper deposition by fluid cooling in intrusion-centered systems: New insights from the Bingham porphyry ore deposit, Utah. *Geology* 32, 217–220.
- Reynolds, T.J., Beane, R.E., 1985. Evolution of hydrothermal fluid characteristics at the Santa Rita, New Mexico, porphyry copper deposit. *Econ. Geol.* 80, 1328–1347.
- Richards, J.P., Spell, T., Rameh, E., Raziq, A., Fletcher, T., 2012. High Sr/Y magmas reflect arc maturity, high magmatic water content, and porphyry Cu ± Mo ± Au potential: examples from the Tethyan arcs of Central and Eastern Iran and Western Pakistan. *Econ. Geol.* 107, 295–332.
- Robert, F., Kelly, W.C., 1987. Ore forming fluids in Archean goldbearing quartz veins in the Sigma Mine, Abitibi greenstone belt, Quebec, Canada. *Econ. Geol.* 82, 1464–1482.
- Roedder, E., 1971. Fluid inclusion studies on the porphyry copper-type ore deposits at Bingham (Utah), Butte (Montana), and Climax (Colorado). *Econ. Geol.* 66, 98–120.
- Rusk, B., Reed, M.H., Dilles, J.H., 2008. Fluid inclusion evidence for magmatic-hydrothermal fluid evolution in the porphyry copper-molybdenum deposit, Butte, Montana. *Econ. Geol.* 103, 307–334.
- Seedorff, E., Dilles, J.H., Proffett, J.M., Einaudi, M.T., Zurcher, L., Stavast, W.J.A., Johnson, D.A., Barton, M.D., 2005. Porphyry deposits: characteristics and origin of hypogene features. *Econ. Geol. 100th Anniversary Volume*, pp. 251–298.
- Shepherd, T., Rankin, A.H., Alderton, D.H.M., 1985. A Practical Guide to Fluid Inclusion Studies. Blackie, London (239 pp.).
- Shinohara, H., 1994. Exsolution of immiscible vapor and liquid phases from a crystallizing silicate melt: implications for chlorine and metal transport. *Geochim. Cosmochim. Acta* 58, 5215–5221.
- Siahcheshm, K., Calagari, A.A., Abedini, A., Lentz, D.R., 2012. Halogen signatures of biotites from the Maher-Abad porphyry copper deposit, Iran: characterization of volatiles in syn- to post-magmatic hydrothermal fluids. *Int. Geol. Rev.* 54, 1353–1368.
- Stöcklin, J., Eftekhamejad, J., Hoshmandzadeh, A., 1971. Initial investigation of central Lut block, eastern Iran. Geological Survey of Iran. 88.
- Tarkian, M., Lotfi, M., Baumann, A., 1983. Tectonic, magmatism and the formation of mineral deposits in the central Lut, east Iran: Ministry of Mines and Metals. Geological Society of Iran, geodynamic project (geotraverse) in Iran, 51 357–383.
- Ulrich, T., Günther, D., Heinrich, C.A., 2001. The Evolution of a porphyry Cu–Au deposit, based on LA-ICP-MS analysis of fluid inclusions: Bajo de la Alumbrera, Argentina. *Econ. Geol.* 96, 1743–1774.
- Ulrich, T., Günther, D., Heinrich, C.A., 2002. The evolution of a porphyry Cu–Au deposit, based on LA-ICP-MS analysis of fluid inclusions: Bajo de la Alumbrera, Argentina. *Econ. Geol.* 97, 1889–1920.
- Vollbrecht, A., 1989. MicroriB-Analyse im KTB-Datenerhebung U-Tisch Mikroskopie. Unpublished Report IGDL, Gottingen.
- Walsh, J.F., Kesler, S.E., Duff, D., Cloke, P.L., 1988. Fluid inclusion geochemistry of high-grade vein-hosted gold ore at the Pamour Mine, Porcupine Camp, Ontario. *Econ. Geol.* 81, 681–703.
- Webster, J.D., Mandeville, C.W., 2007. Fluid immiscibility in volcanic environments. *Rev. Mineral. Geochem.* 65, 313–362.
- Whitney, J.A., 1989. Origin and evolution of silicic magmas: ore deposition associated with magmas. *Rev. Econ. Geol.* 4, 183–201.
- Wilkinson, J.J., 2001. Fluid inclusions in hydrothermal ore deposits. *Lithos* 55, 229–272.
- Zarrinkoub, M.H., Pang, K.N., Chung, S.L., Khatib, M.M., Mohammadi, S.S., Chiu, H.Y., Lee, H.Y., 2012. Zircon U–Pb age and geochemical constraints on the origin of the Birjand ophiolite, Sistan suture zone, eastern Iran. *Lithos* 154, 392–405.